NANO LETTERS
Letter
Cite This: Nano Lett. 2019, 19, 7487−7493
pubs.acs.org/NanoLett

Elaboration of Aggregated Polysulfide Phases: From Molecules to Large Clusters and Solid Phases

Jiewen Xiao,[†] Guangmin Zhou,[‡] Hetian Chen,[†] Xiang Feng,[†] Dominik Legut,[§] Yanchen Fan,[†] Tianshuai Wang,[†] Yi Cui,*[,‡,∥] and Qianfan Zhang*[,†]

[†]School of Materials Science and Engineering, Beihang University, Beijing 100191, P. R. China
[‡]Department of Materials Science and Engineering, Stanford University, Stanford, California 94305, United States
[§]IT4Innovations, VSB-Technical University of Ostrava, 17.listopadu 2172/15, CZ-70800 Ostrava, Czech Republic
[∥]Stanford Institute for Materials and Energy Sciences, SLAC National Accelerator Laboratory, 2575 Sand Hill Road, Menlo Park, California 94025, United States

Supporting Information

ABSTRACT: With the increasing strategies aimed at repressing shuttle problems in the lithium−sulfur battery, dissolved contents of polysulfides are significantly reduced. Except for solid-state Li_2S_2 and Li_2S, aggregated phases of polysulfides remain unexplored, especially in well confined cathode material systems. Here, we report a series of nanosize polysulfide clusters and solid phases from an atomic perspective. The calculated phase diagram and formation energy evolution process demonstrate their stabilities and cohesive tendency. It is interesting to find that Li_2S_6 can stay in the solid state and contains short S_3 chains, further leading to the unique stability and dense structure. Simulated electronic properties indicate reduced band gaps when polysulfides are aggregated, especially for solid phase Li_2S_6 with a band gap as low as 0.47 eV. Their dissolution behavior and conversion process are also investigated, which provides a more realistic model and gives further suggestions on the future design of the lithium−sulfur battery.

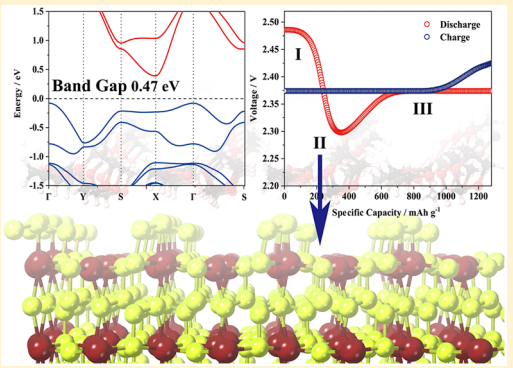

KEYWORDS: *Solid state polysulfides, cohesive tendency, confined cathode system, reduced band gaps, dissolution barrier*

The lithium−sulfur (Li−S) battery, based on the multistep reversible reactions between the lithium metal anode and the sulfur cathode, has emerged as one of the most promising candidates due to its high specific energy density of 2600 Wh/kg.[1] However, the application of the Li−S battery is still hampered by several obstacles, including the insulating nature of the reactants, shuttle problems, capacity attenuation, depletion of electrolytes, and growth of the lithium dendrites.[2,3] One of the most important attributes is the soluble high-order polysulfides, which will inevitably lead to the notorious shuttle problem and impair its long-term electrochemical performance. Therefore, various cathode materials with novel nanosize architectures have been designed,[4,5] focusing on preventing polysulfides from dissolution from the aspects of both physical and chemical confinement, for instance, the core−shell design of transition metal sulfides (TMSs).[6,7] Furthermore, special electrolyte systems with decreased polysulfide solubility have also been reported.[8] Such strategies will effectively suppress the shuttle problem, as verified from both the significantly reduced dissolved polysulfide contents and the discoloration of the polysulfide solution.[7]

Therefore, under the above-mentioned various strategies, polysulfides will be mainly confined in the cathode rather than dissolving into electrolytes. However, a new question arises: the realistic phases of polysulfides in the optimized cathode material system have not been identified and have rarely been considered in previous studies. It can be predicted that the confined cathode system will benefit the interaction among higher-order polysulfides themselves, further resulting in aggregated phases. Traditional approaches treat polysulfides as small molecules,[9,10] whose thermodynamic properties and dissolution behaviors have been identified. The catalytic conversion of polysulfides is also modeled as the transformation of molecular species, while dominant polysulfides are actually restricted in cathodes and exist in complex phases.[11] Nevertheless, systematic research on possible phases of aggregated polysulfides, including nanosize clusters and solid phases, is still lacking. As a result, theoretical understanding of the rational states of lithiated products and their

Received: August 12, 2019
Revised: September 10, 2019
Published: September 11, 2019

DOI: 10.1021/acs.nanolett.9b03297
Nano Lett. 2019, 19, 7487−7493

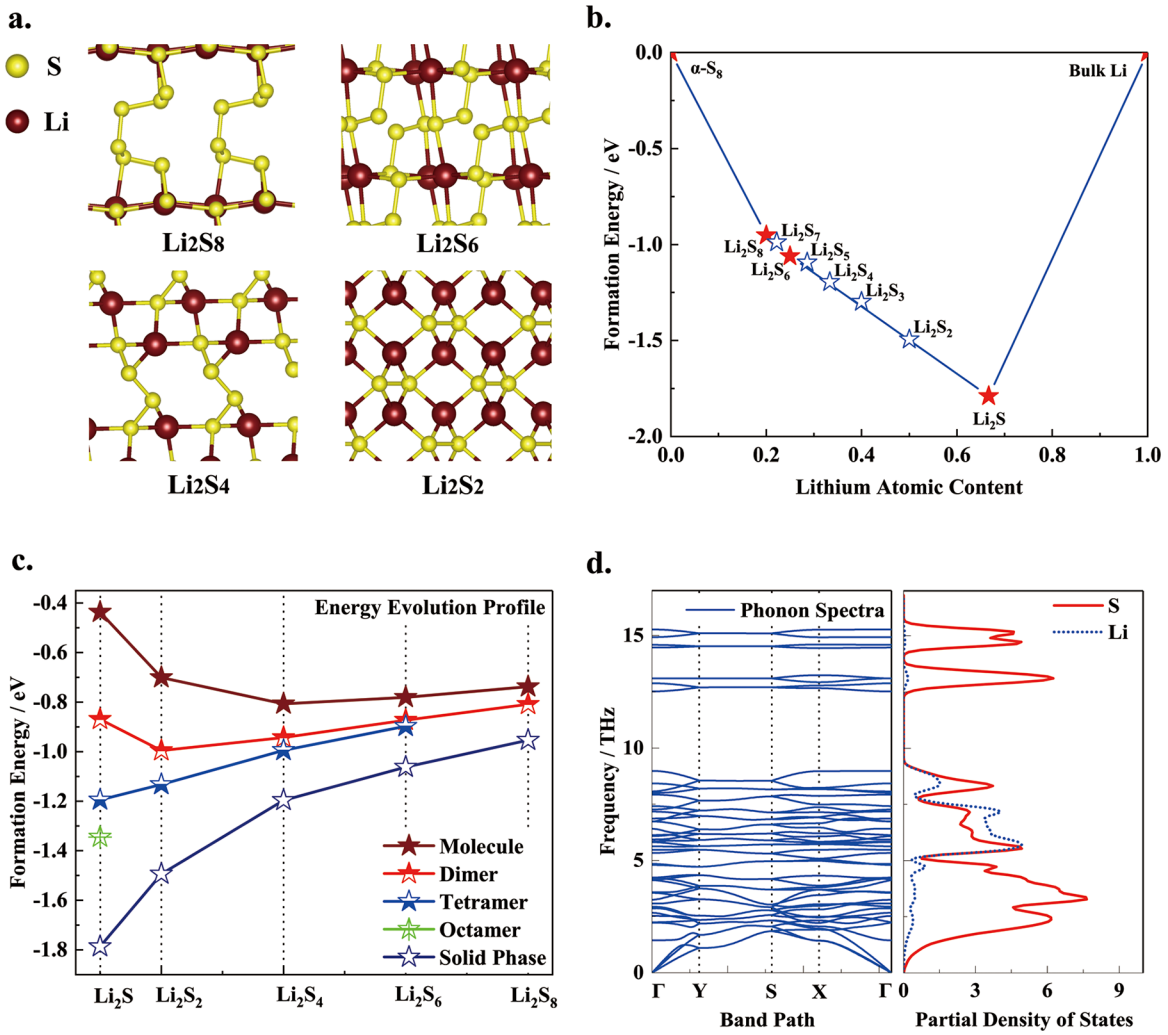

Figure 1. a. Atomic configurations of solid phases of Li_2S_2, Li_2S_4, Li_2S_6, and Li_2S_8. b. Phase diagram of polysulfide solid phases. c. Formation energy evolution profile of different polysulfide phases. d. Simulated phonon spectra and partial density of states of α phase Li_2S_6.

transition process during charge/discharge cycling remains unclear.

In the present work, we systematically elaborated nanosize polysulfide clusters and solid phases from an atomic perspective. Compared to traditional polysulfide molecules, the atomic configurations of polysulfide dimers, tetramers, and solid phases were theoretically clarified. Phase diagrams, energy evolution profiles, and phonon spectra demonstrate their stability and cohesive tendencies. It is found that solid-state Li_2S_6 is the stable phase that only contains a short S_3 chain pattern, being different from the traditional view and endowing it with unique stability. The electronic structure was further analyzed, and we found the reduced band gap of polysulfide solid phases, especially for Li_2S_6 with a band gap as low as 0.47 eV. We further explored their dissolution behavior from both thermodynamics and kinetics, which suggests an impeded dynamic dissolution process of Li_2S_6 due to a large energy barrier. Based on these simulations, we have reexamined the multistep polysulfide conversion processes and clarified the voltage profile detected in experiments.

COMPUTATIONAL METHODS

First-principles calculations were performed using the Vienna *ab initio* simulation package (VASP)[12,13] in the framework of density functional theory (DFT) with projector augmented wave (PAW) pseudopotentials.[14,15] The Perdew−Burke−Ernzerhof (PBE) functional was adopted to describe the exchange-correlation function based on the generalized gradient approximation (GGA).[16] Structure prediction was performed on Crystal Structure Analysis by Particle Swarm Optimization (CALYPSO),[17] to obtain the geometric structures of polysulfide clusters and solid phases. For large polysulfide clusters, we have searched $(Li_2S)_x$ (x = 2, 4, 6, 8), $(Li_2S_n)_x$ (n = 2, 3, 4, 6; x = 2, 4), and the dimers of higher-order Li_2S_8. Since Li_2S is inclined to form large clusters and further be transformed into solid phase, we have simulated the Li_2S clusters up to octamers, while the largest cluster size about other polysulfides (Li_2S_n, n = 2, 3, 4, 6) is up to tetramers. Due to the high solubility of Li_2S_8, only dimers containing 20 atoms are simulated for simplicity. A detailed description of computational methods is shown in the Supporting Information.

RESULTS AND DISCUSSION

I. Geometric Structures and Stability. The atomic configurations of the discovered nanosize polysulfide clusters are presented in Figures S1−S6. For a series of Li_2S clusters, it is found that they generally contain discrete S anions separated

DOI: 10.1021/acs.nanolett.9b03297
Nano Lett. 2019, 19, 7487−7493

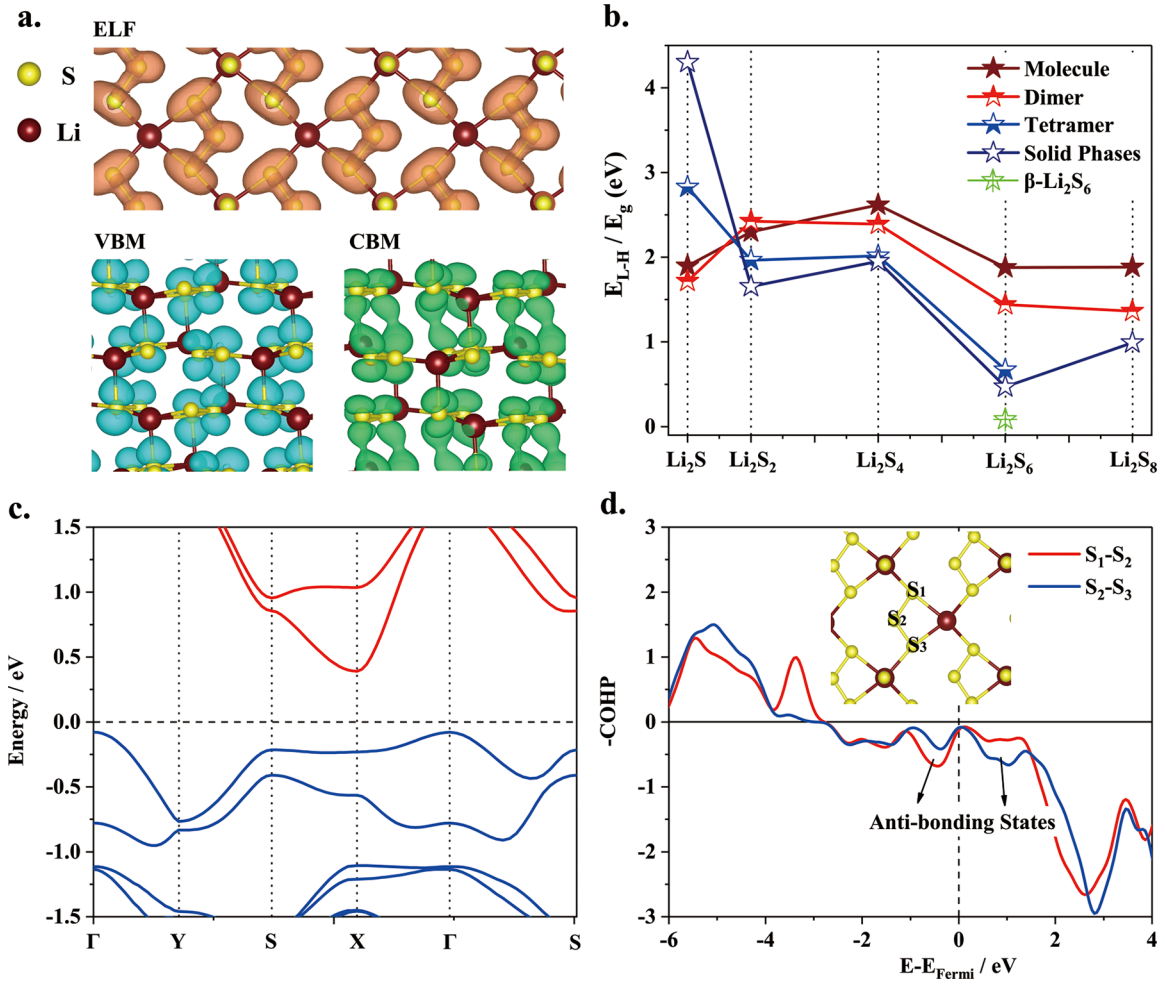

Figure 2. a. ELF, spatial charge distribution of valence band maximum (VBM) and conduction band minimum (CBM) for β-Li_2S_6, with iso-surface value set to 0.700, 0.002, and 0.002 e/Å^3, respectively. b. $E_{L\text{-}H}/E_g$ evolution profile. c. Calculated band structure of β-Li_2S_6 based on HSE scheme. d. COHP analysis for S−S bonds in the S_3 chain of β-Li_2S_6.

by Li ions, similar to the solid bulk phase. For other higher-order polysulfide clusters, a longer sulfur chain appears, whose chain length is consistent with their stoichiometry. Based on the Bader charge analysis, it is revealed that only terminal sulfur in the sulfur chain will acquire considerable electrons from lithium, similar to the case of molecules (Figures S1−S6). Next, for solid phases, the crystalline structures for Li_2S_2, Li_2S_3, Li_2S_4, Li_2S_5, Li_2S_6, and Li_2S_8 are all determined based on similar methods, which have not been systematically clarified yet according to the best of our knowledge. Figure 1a presents the atomic configurations of solid phases of Li_2S_2, Li_2S_4, Li_2S_6, and Li_2S_8, while others are shown in Figure S7, whose lattice parameters, atomic positions, and space groups are collected in Tables S1−S9. Generally, higher-order polysulfides exhibit Li−S networks while S−S chains exist between neighboring planes and further connect with them. Simulated Bader charge in such a geometry shows that transferred charge from lithium to sulfur concentrates on the Li−S plane, and the covalent S chain barely receives electrons from lithium (Figures S4−S6). It is worth noting that, among higher-order solid state polysulfides, only Li_2S_6 possesses short S_3 chains rather than long S_6 chains in the traditional view, endowing it with the highest-density ~1.92 g/cm^3 (Figure S8) and unique dynamic and electronic properties, as shown in the following text.

To identify stable solid phases, we calculated the formation energies for various Li−S species and plotted the phase diagram. As shown in Figure 1b, Li_2S sits in the bottom of the convex hull, with the Li_2S_8 and Li_2S_6 phases being the stable intermediates. There is also a metastable phase of Li_2S_6 with ~4 meV above the hull, and the stable and metastable solid phases of Li_2S_6 are denoted as α and β phases in the following text. Such a trend of the calculated convex hull is the same when applying different vdW methods (Figure S9). Other solid phases, Li_2S_2, Li_2S_3, Li_2S_4, Li_2S_5, and Li_2S_7, are thermodynamically unfavorable However, Li_2S_4 and Li_2S_2 locate very closely to the convex hull, approximately ~10 meV and ~5 meV above. Therefore, Li_2S_4 and Li_2S_2, as metastable intermediates, are also likely to form during discharge, and this may be the primary reason that many experiments can observe these phases. Thus, during the following discussions, we will mainly concentrate on stable phases as Li_2S, Li_2S_6, and Li_2S_8, and metastable phases as Li_2S_2 and Li_2S_4.

The formation energy evolution was further plotted in Figure 1c to show the evolution process from molecules and nanosize clusters to solid phases and from higher-order to lower-order polysulfides. First, for polysulfide molecules, the stability significantly decreases from Li_2S_4 to Li_2S, while higher-order species have similar formation energies. On the other hand, polysulfide tetramers and solid phases exhibit the

DOI: 10.1021/acs.nanolett.9b03297
Nano Lett. 2019, 19, 7487−7493

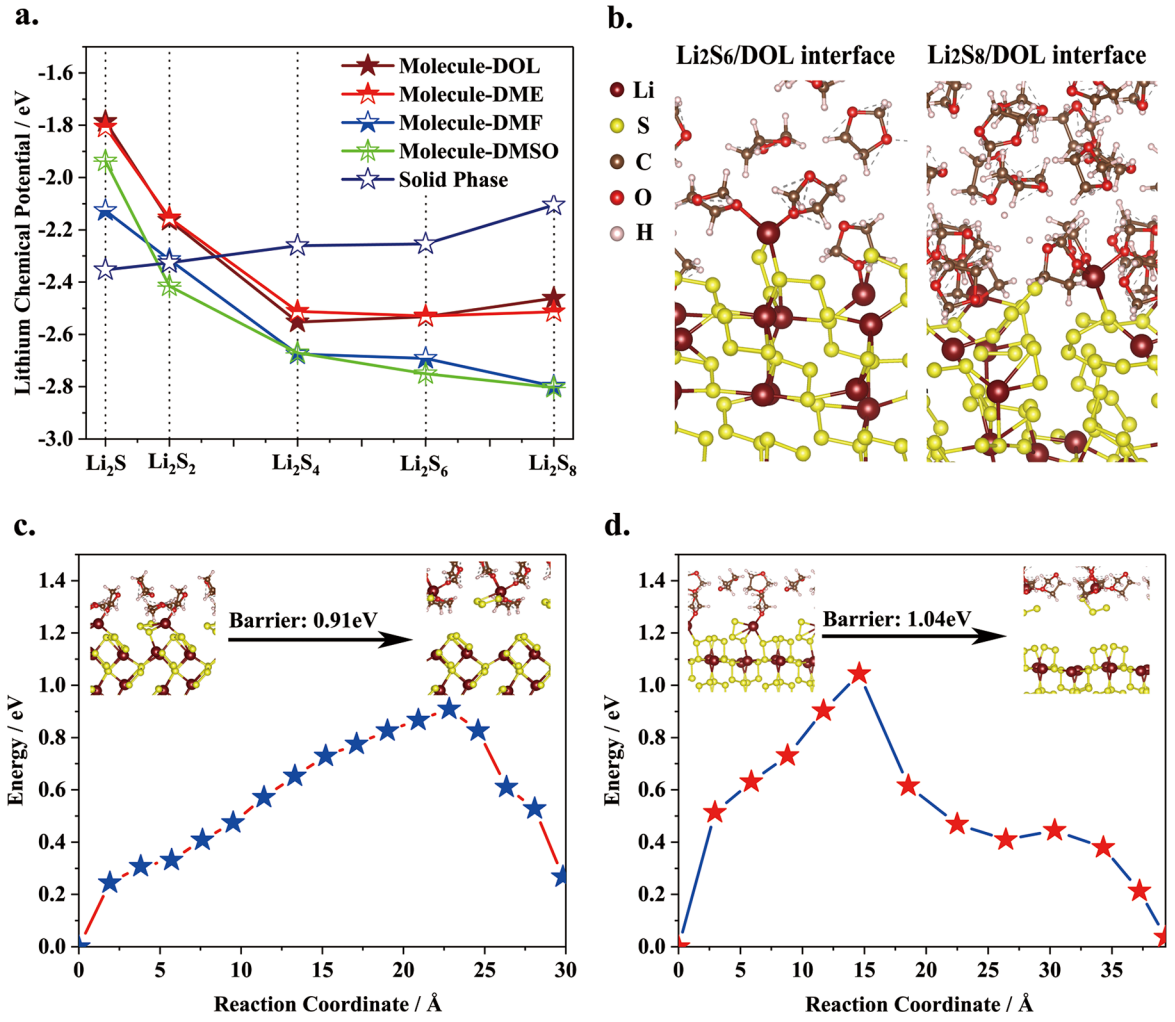

Figure 3. a. Evolution of lithium chemical potential for dissolved polysulfide molecules in different electrolytes and polysulfide solid phases. b. Atomic configuration of Li_2S_6/DOL and Li_2S_8/DOL interface after 20 ps and 10 ps AIMD simulation. Calculated energy evolution profile for the dissolution process on c (001) and d (100) slabs of solid state Li_2S_6, and corresponding initial and final atomic configurations are presented in the inset.

opposite trend: the absolute value of formation energy and thus stability gradually increase when evolving from Li_2S_8 to Li_2S. From the energy evolution profile, we can clarify polysulfides into three categories. The first one contains Li_2S and Li_2S_2, whose molecular phases are highly unstable, and stability will be greatly improved when forming nanosize clusters and solid phases. The second one refers to Li_2S_4 and Li_2S_6, where the formation energy difference between molecular phases and solid phases is around 0.4 eV per atom, denoting a moderate cohesive tendency. The third category only includes Li_2S_8, which exhibits the similar formation energy for molecules, nanosize clusters, and solid phases. Furthermore, solid state Li_2S_8, having a porous structure formed by long S_8 chains, is more like a molecular crystal, which will be easily dissociated into electrolytes (section III).

To demonstrate their dynamical stabilities, phonon spectra were simulated, shown in Figure 1d (α phase Li_2S_6) and Figure S10 (other solid phases). All solid phases lack imaginary modes and possess robust dynamical stability. Partial densities of states (PDOS) were further calculated to analyze the characteristics of Li−S and S−S bonds. For the PDOS of α phase Li_2S_6 in Figure 1d, S−S bond vibration appears at the lower frequency region (0−5 THz), and Li−S bond vibration modes range from 5 to 10 THz, being consistent with previous studies.[18] Such a distribution is a general feature for other solid phases, reflecting the similar bonding types in Li−S species. However, for solid phases of Li_2S_6 with the unique S_3 chain, additional states about the stretching mode of the S_3 unit appear at around 15 THz, yielding the highest vibration frequency.

II. Electronic Properties. Beside their thermodynamic and dynamic stabilities, we further unraveled their electronic properties, and the electronic localization function (ELF) was first analyzed and presented in Figure 2a and Section SIV. With β-Li_2S_6 taken as a typical example, Figure 2a shows that electrons mainly localize around sulfur atoms with the electron localization level around 0.7, reflecting the covalent bond nature. The LUMO−HOMO energy intervals ($E_{L\text{-}H}$) for molecules/clusters and band gaps (E_g) for solid phases are further simulated. It is interesting to find that gaps of Li_2S will be enlarged when going from molecules, through nanosize clusters, and finally to solid phases (Figure 2b). For Li_2S_n (n = 2, 4, 6, 8), the evolution trend is the opposite, where band gaps are reduced when polysulfides are aggregated, especially for α

DOI: 10.1021/acs.nanolett.9b03297
Nano Lett. 2019, 19, 7487−7493

and β phases of Li_2S_6 with band gaps as low as 0.70 and 0.47 eV based on the HSE06 scheme.

Charge density spatial distributions for HOMO/LUMO/CBM/VBM states are presented in Figure 2a (β-Li_2S_6) and Section SIV, exhibiting two kinds of charge spatial distribution depending on the existence of sulfur chain. For $(Li_2S)_x$ (x = 1, 2, 4, 8), HOMO states are contributed from discrete p orbitals of sulfur due to the lack of a sulfur chain, while LUMO states mainly concentrate on lithium atoms with delocalized feature. For sulfur-chain-containing systems, HOMO/VBM and LUMO/CBM are dominantly distributed on different parts of the S chain (Figure 2a and S12−S19). For instance, in solid phases, VBM states concentrate on the Li−S interconnected plane, and CBM states belong to the interplanar sulfur chain. Therefore, charge transfer from VBM to CBM in these solid phases is spatially separated, leading to poor conductivity accordingly. In contrast, edge states for the two solid phases of Li_2S_6 are quite different due to their unique S_3 chain pattern. For β phase Li_2S_6, both CBM and VBM exhibit the characteristics of anti-π bonds, which are composed of p_z states of sulfur perpendicular to the (100) Li−S plane (Figure 2a). The α phase has a similar but less remarkable distribution feature (Figure S16). Crystal Occupation Hamilton Population (COHP) evaluation was performed to investigate the S−S bonds of the S_3 chain in β-Li_2S_6. As shown in Figure 2d, it can be observed that such symmetric S_3 chains will result in two close antibonding states around the Fermi level for both S_1−S_2 and S_2−S_3 bonds, leading to the smallest band gap of 0.47 eV accordingly.

III. Dissolution Behaviors: Thermodynamics and Kinetics. After identifying their geometric and electronic properties, dissolution behavior was further explored. Here, we have mainly considered polysulfide−dimethoxyethane (DME)[19]/dioxolane (DOL)[20] systems, which are most commonly adopted in experiments. Dimethylformamide (DMF) and dimethyl sulfoxide (DMSO) solvents with high donor number and dielectric constant[21] are also investigated to demonstrate the reasonability of our model. To compare the stability of dissolved molecules, nanosize clusters, and solid polysulfides, lithium chemical potential is applied. More detailed descriptions are shown in the Supporting Information.

The evolution of lithium chemical potential at different lithiation stages is presented in Figure 3a. For polysulfide molecules, we have tested DME/DOL/DMF/DMSO electrolyte systems, exhibiting two kinds of evolution processes. For the DME/DOL system, polysulfide molecules Li_2S_n ($n \geq 4$) are more stable than the solid intermediates since the formation of the Li−O bond greatly deforms their atomic structure. For Li_2S_2 and Li_2S, dissolved molecules still possess higher energy than their solid phases, consistent with the phase transition during lithiation stages. On the other hand, for DMF/DMSO systems, the enhanced dielectric constant increases the solubility of polysulfides, particularly for Li_2S_8. Furthermore, solid state Li_2S_2 can also be slightly soluble in DMSO, in accordance with the detected solubility of Li_2S_2 in DMSO.[22] Next, compared to molecular phases, the lithium chemical potential of polysulfide nanosize clusters falls into the intermediate region between corresponding bulk phases and molecules, as expected (Figure S20). Generally, for the three categories of polysulfides as mentioned in section II, different dissolution behaviors are exhibited: (1) solid phases Li_2S and Li_2S_2 are more stable than dissolved molecules and clusters; (2) Li_2S_4 and Li_2S_6 have moderate thermodynamic dissolution tendency; (3) Li_2S_8 possesses high solubility since dissolved dimers and molecules of Li_2S_8 have similar μ_{Li} that is much lower than solid phases. The above classification is also suggested by the solubility detected in experiments: for Li_2S_6, the solubility in DOL/DME is only around 1 M/L, while Li_2S_4 is more insoluble than Li_2S_6; both are far below the value ∼6 M/L for Li_2S_8.[22]

Except for thermodynamic simulations, we further explored their kinetic behaviors. Here, the *ab initio* molecular dynamics (AIMD) simulation was applied to investigate the interfaces formed by DOL solvents and two kinds of typical intermediates as solid state Li_2S_6 and Li_2S_8. Snapshots of the AIMD simulations after 20 ps are shown in the left panel of Figure 3b. It indicates the deformed surface of the Li_2S_6 slab, while the whole atomic structure still holds together without observing the dynamic dissolution process. Similar to Li_2S_6, the dynamic behavior for the (001) slab of Li_2S_8 was also studied. Figure 3b shows the atomic configuration of the Li_2S_8/DOL electrolyte interface after 10 ps. It can be clearly seen that the thin Li−S plane is deformed severely along with the dissociation of the long S_8 chain. Furthermore, the kinetic behavior for the polysulfides/DME interface is also explored (Figure S21), which exhibits the same behaviors as that in DOL, further verifying the similar thermodynamic and kinetic polysulfide dissolution behaviors for polysulfides in both DME and DOL solvents.[23] Therefore, AIMD simulation demonstrates that the dissolution of Li_2S_8 can easily happen, while for aggregated Li_2S_6, it may possess a certain stability against dissolution. To quantitatively describe the dissolution impedance, the climbing image-nudged elastic band (CI-NEB) methods were further applied for the polysulfides/DOL interface. The energy evolution profiles for the dissolution process are shown in Figure 3c and d for (001) and (100) slabs of Li_2S_6, respectively. Results indicate that the dissolution energy barrier is 0.91 and 1.04 eV for (001) and (100) surfaces, which is a sizable value and illustrates the observations during AIMD simulation. To conclude, thermodynamic calculation about the lithium chemical potential verifies the observed solubility of polysulfides in experiments. However, kinetic simulations reveal that the dissolution of solid state Li_2S_6 in DOL/DME electrolyte will be impeded by a sizable energy barrier, while solid state Li_2S_8 is highly unstable against dissolution.

IV. Polysulfide Conversion: Voltage Profile for Discharge/Charge. Based on the dissolution process, we can thus describe the voltage evolution in a confined cathode system. Since Li_2S_8 exhibits considerable dissolution tendency and strong molecular features, it is treated as dissolved molecules, and Li_2S_2 and Li_2S are considered as solid phases. On the other hand, the second category, Li_2S_6 and Li_2S_4, has a sizable dissolution energy barrier and moderate cohesive tendency, and the formation of solid phases will be further enhanced in the optimized cathode system. Therefore, they are modeled as solid phases confined in cathode materials.

The phase transition for the charge/discharge process can be illustrated as Figure 4a while the corresponding voltage evolution profile is presented in Figure 4b and Table 1. The discharge process can go on in the following pathway: (1) soluble Li_2S_8 is formed in the first plateau with voltage 2.49 V. (2) Li_2S_8 is transformed to aggregated solid state Li_2S_6 and Li_2S_4 along with the formation of Li_2S_2 and Li_2S. This region corresponds to the transitional stage with voltages ranging from 2.29 to 2.10 V. It is worth noting that dissolved Li_2S_8

DOI: 10.1021/acs.nanolett.9b03297
Nano Lett. 2019, 19, 7487−7493

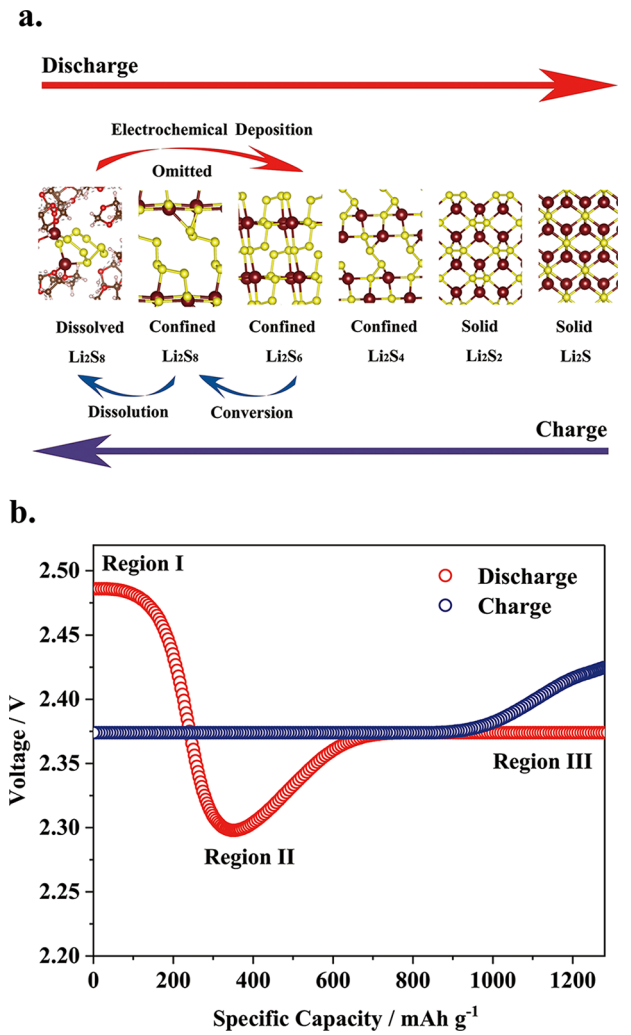

Figure 4. a. Schematic representation of discharge/charge mechanism in the optimized cathode system. b. Corresponding voltage profiles based on Table 1. Regions I, II, and III are classified based on discharge and will be reversed for the charge process.

tends to dissociate into higher-order polysulfides (Li_2S_6 and Li_2S_4) and Li_2S_2 and Li_2S at the same time, as this is more thermodynamically favorable than only forming Li_2S_4 and Li_2S_6 species. Experimental observation that Li_2S appears at the initial stage of the second plateau further verifies our approach.[24] Due to the conversion from the dissolved molecular structure into confined solid phases, the voltage in this stage is relatively lower, thus reproducing the dip in the voltage profile observed in the experiments.[25,26] (3) Confined solid phases (Li_2S_6 and Li_2S_4) are further converted to Li_2S_2 and the final discharge product Li_2S with voltage ~2.37 V. Solid phase conversion in this stage would be sluggish and induce overpotentials, so the calculated value is higher than that in the experiments. For the charge process, the differences occur in region II, where liquid−solid transformation happens. As shown in Figure 4a and Table 1, the flat voltage plateau was maintained since solid state Li_2S_8 was involved in the electrochemical process and is responsible for the voltage in this region. Then, spontaneous dissolution happens, producing dissolved reactants in region I, while for discharging, the solid state Li_2S_8 phase is missed and the electrochemical deposition of dissolved species induces the voltage dip. Therefore, the

Table 1. Discharge and Charge Processes of Li−S Batteries when Polysulfides Are Confined in the Optimized Cathode System[a]

region	reaction	phases	voltage/V
I	$S_8 + 2Li \rightarrow Li_2S_8$*	**Dissolved molecules**	2.49
II	**Discharge**	Li_2S_8	
	Li_2S_8* + $2Li \rightarrow Li_2S_6 + Li_2S_2$		2.10
	Li_2S_8* + $4Li \rightarrow Li_2S_6 + 2Li_2S$		2.24
	Li_2S_8* + $4Li \rightarrow Li_2S_4 + 2Li_2S_2$		2.21
	Li_2S_8* + $8Li \rightarrow Li_2S_4 + 4Li_2S$		2.29
	Charge	**Confined Solid Phases**	
	$Li_2S_6 + 2Li_2S \rightarrow Li_2S_8 + 4Li$	Li_2S_6, Li_2S_4	2.42
	$Li_2S_6 + Li_2S_2 \rightarrow Li_2S_8 + 2Li$		2.47
	$Li_2S_4 + 4Li_2S \rightarrow Li_2S_8 + 8Li$		2.39
	$Li_2S_4 + 2Li_2S_2 \rightarrow Li_2S_8 + 4Li$		2.40
III	$Li_2S_6 + 2Li \rightarrow Li_2S_4 + Li_2S_2$		2.33
	$Li_2S_6 + 4Li \rightarrow Li_2S_4 + 2Li_2S$		2.35
	$Li_2S_6 + 4Li \rightarrow 3Li_2S_2$	**Solid Phases**	2.36
	$Li_2S_6 + 10Li \rightarrow 6Li_2S$	Li_2S_2, Li_2S	2.37
	$Li_2S_4 + 2Li \rightarrow 2Li_2S_2$		2.39
	$Li_2S_4 + 6Li \rightarrow 4Li_2S$		2.38
	$Li_2S_2 + 2Li \rightarrow 2Li_2S$		2.37

[a] Li_2S_8* denotes dissolved states while Li_2S_8 represents solid phases.

characteristics on the two plateaus of discharge and one flat plateau of charge can be clarified from a thorough theoretical perspective.

Finally, we will give some further suggestions on the future design of Li−S batteries. First, the dissolution process will lead to the different characteristics of discharge and charge, and further impair the long-term cycling performance. A successful repression of dissolution will ameliorate the dip in discharge and further produce the flat voltage profile, as demonstrated by Nazar et al. in experiments.[8] Such modification on the voltage dip of the discharge voltage profile can be used to evaluate the effectiveness of prevention on polysulfide dissolution. Second, to guide operando experiments for detecting polysulfides in a confined cathode system, Raman spectra were further calculated and shown in section SVI. Third, we have taken graphene as a typical example and calculated the binding energies toward Li_2S molecules, dimers, tetramers, octamers, and slabs of solid phase, which verifies that the aggregated phase would be more stable and reasonable when considering polysulfides/loading material interactions (section SVII). Therefore, the further exploration of polysulfide conversion among aggregated phases will serve as theoretical guidance for future cathode material design in the Li−S battery.

CONCLUSION

In conclusion, we have systematically identified polysulfide clusters and solid phases, whose geometric structure, stability, and electronic properties are elaborated. Phase diagram and formation energy evolution reveal stable solid phases as Li_2S_8 and Li_2S_6 and metastable phases as Li_2S_4 and Li_2S_2, which all possess excellent dynamical stabilities. Electronic structures indicate that aggregated polysulfide clusters and solid phases have reduced band gaps, which is most remarkable for β-Li_2S_6 with a band gap as low as 0.47 eV. Furthermore, we have simulated the dissolution process and found that Li_2S_6 possesses a sizable dissolution energy barrier although it

DOI: 10.1021/acs.nanolett.9b03297
Nano Lett. 2019, 19, 7487−7493

tends to dissolve thermodynamically. Under the confined cathode material system, we have finally proposed the corresponding lithiation/delithiation process based on multistep conversions among polysulfide solid phases, being consistent with experiments. This work not only elaborates various polysulfide species, but also illustrates their dissolution behavior and multistep conversions, shedding light on understanding complex reactions in the Li−S battery.

■ ASSOCIATED CONTENT

Supporting Information

The Supporting Information is available free of charge on the ACS Publications website at DOI: 10.1021/acs.nanolett.9b03297.

Detailed description of computational methods; Geometric structures, dynamic stabilities and electronic structure of polysulfide clusters and solid phases; Additional simulations for dissolved polysulfides in DOL and DME electrolyte; Simulated Raman spectra; Binding strength of graphene toward different phases of polysulfides (PDF)

■ AUTHOR INFORMATION

Corresponding Authors

*E-mail: qianfan@buaa.edu.cn.
*E-mail: yicui@stanford.edu.

ORCID

Jiewen Xiao: 0000-0002-6686-3867
Guangmin Zhou: 0000-0002-3629-5686
Hetian Chen: 0000-0003-4505-403X
Tianshuai Wang: 0000-0002-9453-0090
Yi Cui: 0000-0002-6103-6352
Qianfan Zhang: 0000-0001-8121-7727

Notes

The authors declare no competing financial interest.

■ ACKNOWLEDGMENTS

Q.F.Z. was supported by National Key Research and Development Program of China (No. 2017YFB0702100) and National Natural Science Foundation of China (11404017). Y.C. was supported by the Assistant Secretary for Energy Efficiency and Renewable Energy, Office of Vehicle Technologies of the U.S. Department of Energy, under the Battery Materials Research program and the Battery 500 Consortium program. D.L. acknowledges support by the European Regional Development Fund in the IT4Innovations national supercomputing center-Path to Exascale project, No. CZ.02.1.01/0.0/0.0/16_013/0001791 within the Operational Programme Research, Development and Education and by the Ministry of Education by Czech Science Foundation project No. 17-27790S, and grant No. 8J18DE004 of Ministry of Education, Youth, and Sport of the Czech Republic.

■ REFERENCES

(1) Fan, Y.; Chen, X.; Legut, D.; Zhang, Q. *Energy Storage Mater.* **2019**, *16*, 169−193.
(2) Gu, S.; Sun, C.; Xu, D.; Lu, Y.; Jin, J.; Wen, Z. *Electrochem. Energy Rev.* **2018**, *1*, 599−624.
(3) Cheng, X.-B.; Huang, J.-Q.; Zhang, Q. *J. Electrochem. Soc.* **2018**, *165* (1), A6058−A6072.
(4) Seh, Z. W.; Sun, Y.; Zhang, Q.; Cui, Y. *Chem. Soc. Rev.* **2016**, *45*, 5605.
(5) Li, Y.; Wang, W.; Liu, X.; Mao, E.; Wang, M.; Li, G.; Fu, L.; Li, Z.; Eng, A. Y. S.; Seh, Z. W.; Sun, Y. *Energy Storage Mater.* **2019**, DOI: 10.1016/j.ensm.2019.05.005.
(6) Seh, Z. W.; Li, W.; Cha, J. J.; Zheng, G.; Yang, Y.; McDowell, M. T.; Hsu, P.; Cui, Y. *Nat. Commun.* **2013**, *4*, 1331.
(7) Seh, Z. W.; Yu, J. H.; Li, W.; Hsu, P.; Wang, H.; Sun, Y.; Yao, H.; Zhang, Q.; Cui, Y. *Nat. Commun.* **2014**, *5*, 5017.
(8) Pang, Q.; Shyamsunder, A.; Narayanan, B.; Kwok, C. Y.; Curtiss, L. A.; Nazar, L. F. *Nat. Energy* **2018**, *3*, 783−791.
(9) Zhou, G.; Tian, H.; Jin, Y.; Tao, X.; Liu, B.; Zhang, R.; Seh, Z. W.; Zhuo, D.; Liu, Y.; Sun, J.; Zhao, J.; Zu, C.; Wu, D. S.; Zhang, Q.; Cui, Y. *Proc. Natl. Acad. Sci. U. S. A.* **2017**, *114*, 840−845.
(10) Du, Z.; Chen, X.; Hu, W.; Chuang, C.; Xie, S.; Hu, A.; Yan, W.; Kong, X.; Wu, X.; Ji, H.; Wan, L. *J. Am. Chem. Soc.* **2019**, *141*, 3977−3985.
(11) Gao, G.; Zheng, F.; Pan, F.; Wang, F. *Adv. Energy Mater.* **2018**, *8*, 1801823.
(12) Kresse, G.; Furthmuller, J. *Comput. Mater. Sci.* **1996**, *6*, 15.
(13) Kresse, G.; Furthmuller, J. *Phys. Rev. B: Condens. Matter Mater. Phys.* **1996**, *54*, 11169.
(14) Blochl, P. E. *Phys. Rev. B: Condens. Matter Mater. Phys.* **1994**, *50*, 17953.
(15) Kresse, G.; Joubert, D. *Phys. Rev. B: Condens. Matter Mater. Phys.* **1999**, *59*, 1758.
(16) Perdew, J. P.; Burke, K.; Ernzerhof, M. *Phys. Rev. Lett.* **1996**, *77*, 3865.
(17) Wang, Y.; Lv, J.; Zhu, L.; Ma, Y. *Comput. Phys. Commun.* **2012**, *183*, 2063.
(18) Pan, Y.; Guan, W. M. *Inorg. Chem.* **2018**, *57*, 6617−6623.
(19) Henderson, W. A. *J. Phys. Chem. B* **2006**, *110*, 13177−13183.
(20) Peled, E.; Sternberg, Y.; Gorenshtein, A.; Lavi, Y. *J. Electrochem. Soc.* **1989**, *136*, 1621−1625.
(21) Cuisinier, M.; Hart, C.; Balasubramanian, M.; Garsuch, A.; Nazar, L. F. *Adv. Energy Mater.* **2015**, *5*, 1401801.
(22) Pan, H.; Wei, X.; Henderson, W. A.; Shao, Y.; Chen, J.; Bhattacharya, P.; Xiao, J.; Liu, J. *Adv. Energy Mater.* **2015**, *5*, 1500113.
(23) Kamphaus, E. P.; Balbuena, P. B. *J. Phys. Chem. C* **2017**, *121*, 21105−21117.
(24) Walus, S.; Barchasz, C.; Colin, J.; Martin, J.; Elkaim, E.; Lepretre, J.; Alloin, F. *Chem. Commun.* **2013**, *49*, 7899−7901.
(25) Cuisinier, M.; Cabelguen, P.-E.; Adams, B. D.; Garsuch, A.; Balacubramanian, M.; Nazar, L. F. *Energy Environ. Sci.* **2014**, *7*, 2697−2705.
(26) Wujcik, K. H.; Velasco-Velez, J.; Wu, C. H.; Pascal, T.; Teran, A. A.; Marcus, M. A.; Cabana, J.; Guo, J.; Prendergast, D.; Salmeron, M.; Balsara, N. P. *J. Electrochem. Soc.* **2014**, *161*, A1100−A1106.

DOI: 10.1021/acs.nanolett.9b03297
Nano Lett. 2019, 19, 7487−7493